

# Modeling of the Melting Point, Debye Temperature, Thermal Expansion Coefficient, and the Specific Heat of Nanostructured Materials

Y. F. Zhu, J. S. Lian, and Q. Jiang\*

Key Laboratory of Automobile Materials, Ministry of Education and School of Materials Science and Engineering, Jilin University, Changchun 130022, China

Received: March 2, 2009; Revised Manuscript Received: July 28, 2009

The size-dependences of the melting point, Debye temperature, thermal expansion coefficient, and the specific heat of nanostructured materials have been modeled free of adjustable parameters. The melting point and Debye temperature drop while the thermal expansion coefficient and specific heat rise when the grain size is decreased. Relative to nanoparticles, however, the variation of the above parameters of nanostructured material is weak, dominated by the ratio of the grain boundary energy to the surface energy. Our theoretical predictions agree fairly well with available experimental and computer simulation results for semiconductors and metals.

## 1. Introduction

Size-dependent properties of nanoparticles (NPs) and nanostructured materials (NSs) are one of the most important foundations of nanoscience and nanotechnology.<sup>1,2</sup> Evidence<sup>3–6</sup> shows that the physical and chemical properties of NPs and NSs differ from their bulk counterparts. For example, the melting point  $T_m(D)$ <sup>7–11</sup> and the Debye temperature  $\theta_D(D)$ <sup>12,13</sup> of NPs and NSs drop with  $D$ , where  $D$  denotes the diameter of NPs or grain size of NSs. In contrast, the amplitude of thermal vibration  $\sigma(T,D)$ ,<sup>12</sup> the thermal expansion coefficient  $\alpha(T,D)$ ,<sup>2,14</sup> and the specific heat  $C_p(T,D)$ <sup>15,16</sup> increase, with  $T$  being the absolute temperature. These changes are relevant to the increased surface (interface)/volume ratio, or the atomic coordination imperfection induced by the significant amount of atoms at the surface or interface, whose thermal vibrational energy is larger than that of the interior case.<sup>17–19</sup> However, the variation of these parameters of NSs is found somewhat weaker than that of NPs. According to computer simulation results, for example,  $T_m(D)$  of Ag is depressed from 1149 to 1044 K for NSs but from 1130 to 933 K for NPs when  $D$  drops from 12.12 to 3.03 nm.<sup>10,11</sup> Understanding the size-dependent properties of NPs and NSs due to distinct surface (interface) states will provide the critical information for architecture designs of the next generation of electronic and mechanical devices.

The above phenomena have been modeled in particular for the  $T_m(D)$  of NPs.<sup>1,20,21</sup> Thermodynamically, the classical capillary theory describes the capillary pressure difference sustained across the interface between two static fluids due to the effect of surface tension.<sup>23</sup> In light of it, the well-known Gibbs–Thomson equation was developed to elucidate the function of  $T_m^{\text{NP}}(D)$ ,<sup>24,25</sup> which is expressed as

$$T_m^{\text{NP}}(D)/T_m(\infty) = 1 - 4[\gamma_{\text{sv}}(\infty) - \gamma_{\text{lv}}(\infty)(\rho_s/\rho_l)^{2/3}] \times V_s/[DH_m(\infty)] \quad (1)$$

where  $\infty$  denotes the bulk size;  $V_s$ , the molar volume of the solid phase; and  $H_m$ , the latent heat of fusion.  $\gamma_{\text{sv}}$  and  $\gamma_{\text{lv}}$  denote the respective energies of the solid–vapor and liquid–vapor

interfaces, and  $\rho_s$  and  $\rho_l$  are the respective densities of the solid and liquid phases. Since  $\rho_s \approx \rho_l$ ,  $(\rho_s/\rho_l)^{2/3} \approx 1$ , and  $\gamma_{\text{sv}}(\infty) - \gamma_{\text{lv}}(\infty) \approx \gamma_{\text{sl}}(\infty)$  for the most cubic metals where  $\gamma_{\text{sl}}$  is the solid–liquid interface energy. Equation 1 can thus be newly given as  $T_m^{\text{NP}}(D)/T_m(\infty) = 1 - 4\gamma_{\text{sl}}(\infty)V_s/DH_m(\infty)$ , where  $\gamma_{\text{sl}}(\infty) = [2S_{\text{vib}}(\infty)H_m(\infty)h]/3V_sR$ , with  $S_{\text{vib}}$  being the vibrational contribution of overall melting entropy of the bulk crystals;  $R$ , the ideal gas constant; and  $h$ , the atomic diameter.<sup>26</sup> Since  $\gamma_{\text{sl}}(D)$  and  $H_m(D)$  are size-dependent, where both of them are suppressed as  $D$  is reduced,<sup>26,27</sup> eq 1 is further modified as  $T_m^{\text{NP}}(D)/T_m(\infty) = 1 - 4\gamma_{\text{sl}}(D)V_s/DH_m(D)$  with  $\gamma_{\text{sl}}(D) = [2S_{\text{vib}}(D)H_m(D)h]/3V_sR$ . Substituting the  $\gamma_{\text{sl}}(D)$  relation into it, one has  $T_m^{\text{NP}}(D)/T_m(\infty) = 1 - 8hS_{\text{vib}}(D)/3RD$ .  $S_{\text{vib}}(D)$  is a weak function of  $D$ , which could even be ignored as a first-order approximation.<sup>20</sup> Associated with it, the size-dependence of  $\gamma_{\text{sl}}(D)/H_m(D)$  is negligible. In light of the above discussion, for simplification, eq 1 is rewritten as

$$T_m^{\text{NP}}(D)/T_m(\infty) = 1 - 8hS_{\text{vib}}(\infty)/3RD \quad (2)$$

Equation 2 reasonably matches the experimental data with  $D \geq 10$  nm where the crystal retains its bulk values of  $\gamma_{\text{sl}}$ ,  $H_m$ , and  $S_{\text{vib}}$ .<sup>24,25,28</sup> However, it fails for nanocrystals with  $D < 10$  nm and cannot explain the dimension effect, which will be discussed later.

On the basis of Lindemann's criterion and Mott's expression of the vibrational entropy, a new formula to describe  $T_m^{\text{NP}}(D)$  has been proposed as<sup>29–31</sup>

$$T_m^{\text{NP}}(D)/T_m(\infty) = \exp[-(\alpha_{\text{NP}} - 1)/(D/D_0 - 1)] \quad (3)$$

with  $\alpha_{\text{NP}} = \sigma_{\text{sv}}(T_m, D)^2/\sigma_{\text{in}}(T_m, D)^2 = 2S_{\text{vib}}(\infty)/3R + 1$  where  $\sigma^2$  is the mean square displacement of thermal vibration at  $T = T_m$ , the subscripts sv and in denote the surface and interior atoms. In eq 3,  $D_0 = 2(3 - d)h$  where almost all atoms or molecules are located on the surface and a crystalline structure is no longer stable,<sup>29</sup>  $d$  denotes the dimension of the crystal with  $d = 0$  for nanoparticles,  $d = 1$  for nanowires, and  $d = 2$  for thin films.

\* Corresponding author. Fax: 86-431-85095876. E-mail: jiangq@jlu.edu.cn.

However, models for the size-dependent thermodynamic properties of NSs remain unavailable. As results, one approximately takes the size-dependent properties of NPs in terms of eq 3 as that of NSs. In fact, the size-dependent melting temperature,  $T_m^{NS}(D)$ , for NSs is a weaker function of  $D$  than  $T_m^{NP}(D)$ , since the atomic cohesive energy at grain boundaries is higher than that at free surfaces. A new quantitative description of  $T_m^{NS}(D)$  is therefore expected. Note that this modeling will also help us understand the relationship between the Gibbs–Thompson equation and the melting behaviors of NSs.

In this contribution,  $T_m(D)$ ,  $\theta_D(D)$ ,  $\alpha(T, D)$ , and  $C_p(T, D)$  functions of NSs are modeled. All these functions will be compared with available experimental or computer simulation results.

## 2. Model

Although NSs and NPs have different interfaces on their boundaries (namely, grain boundaries and free surfaces), NSs have crystalline structures that are similar to NPs. Therefore,  $T_m^{NS}(D)$  can be explored by using a modification of eq 3 as

$$T_m^{NS}(D)/T_m(\infty) = \exp[-(\alpha_{NS} - 1)/(D/D_0 - 1)] \quad (4)$$

where  $\alpha_{NS} = \sigma_{gb}(T_m, D)^2/\sigma_{in}(T_m, D)^2$  with the subscript gb denoting the atoms at grain boundaries, which is the only difference between eqs 3 and 4.

Knowing that  $\sigma^2 \propto 1/E_c$ , where  $E_c$  is the mean atomic cohesive energy,<sup>29</sup> one has the relations of  $E_{csv}(\infty) \propto 1/\sigma_{sv}(T_m, \infty)^2$  and  $E_{cin}(\infty) \propto 1/\sigma_{in}(T_m, \infty)^2$ . Because  $E_{cin}(\infty) - E_{csv}(\infty) \propto \gamma_{sv}(\infty)$ ,<sup>32</sup> it says  $1/\sigma_{in}(T_m, \infty)^2 - 1/\sigma_{sv}(T_m, \infty)^2 \propto \gamma_{sv}(T_m, \infty)$  at surfaces of bulk crystals. In analogy to this relationship, it reads  $1/\sigma_{in}(T_m, \infty)^2 - 1/\sigma_{gb}(T_m, \infty)^2 \propto \gamma_{gb}(\infty)$  at grain boundaries of bulk crystals with  $\gamma_{gb}(\infty)$  being the grain boundary energy. Combining these two equations, we get  $[1 - \sigma_{in}(T_m, \infty)^2/\sigma_{gb}(T_m, \infty)^2]/[1 - \sigma_{in}(T_m, \infty)^2/\sigma_{sv}(T_m, \infty)^2] = \gamma_{gb}(\infty)/\gamma_{sv}(\infty)$ . On the basis of the assumption that  $\sigma_{sv}(T_m, \infty)^2/\sigma_{in}(T_m, \infty)^2 = \sigma_{sv}(T_m, D)^2/\sigma_{in}(T_m, D)^2 = \alpha_{NP}$  is size-independent in eq 3, although  $\sigma_{sv}(T_m, D)^2$  and  $\sigma_{in}(T_m, D)^2$  are size-dependent,<sup>31</sup>  $\sigma_{gb}(T_m, \infty)^2/\sigma_{in}(T_m, \infty)^2 = \sigma_{gb}(T_m, D)^2/\sigma_{in}(T_m, D)^2 = \alpha_{NS}$  is also supposed for NSs. Inserting these two assumptions into the above combined equation, one has  $(1 - 1/\alpha_{NS})/(1 - 1/\alpha_{NP}) = \gamma_{gb}(\infty)/\gamma_{sv}(\infty)$  or  $\alpha_{NS} = \gamma_{sv}(\infty)\alpha_{NP}/\{\gamma_{gb}(\infty) + [\gamma_{sv}(\infty) - \gamma_{gb}(\infty)]\alpha_{NP}\}$ . Substituting it into eq 4,  $T_m^{NS}(D)$  is shown as

$$T_m^{NS}(D)/T_m(\infty) = \exp[-\delta(\alpha_{NP} - 1)/(D/D_0 - 1)] \quad (5)$$

where  $\delta = 1/\{1 + [\gamma_{sv}(\infty)/\gamma_{gb}(\infty) - 1]\alpha_{NP}\}$  is an additional term induced by the difference between surfaces and grain boundaries. Note that since  $\gamma_{sv}(\infty) > \gamma_{gb}(\infty)$ ,  $\delta < 1$ , and  $T_m^{NS}(D) > T_m^{NP}(D)$  is thus expected. In eq 5,  $\gamma_{gb}(\infty)$  and  $\gamma_{sv}(\infty)$  functions have been theoretically explored.<sup>26</sup> For the size range of the Gibbs–Thompson equation with  $D > 10$  nm, on the basis of a mathematical relationship of  $\exp(-x) \approx 1 - x$  with small  $x$  value, eq 5 is simplified as  $T_m^{NS}(D)/T_m(\infty) \approx 1 - \delta(\alpha_{NP} - 1)D_0/D = 1 - \delta[2S_{vib}(\infty)D_0/3RD]$ , which is very similar to eq 2. Considering that the Gibbs–Thompson equation has neglected the dimension effect, a middle dimension of  $d = 1$  is taken as a good approximation among  $d = 0, 1$ , and 2, and  $D_0 = 4h$  is thus taken. In view of these considerations, an extended Gibbs–Thompson equation for NSs can be rewritten as

$$T_m^{NS}(D)/T_m(\infty) = 1 - \delta[8hS_{vib}(\infty)/3RD] \quad (6)$$

Equation 6 reflects that eq 5 can be considered as an equivalent or an extension of the Gibbs–Thompson equation for NSs.

On the basis of the proportional relationship of  $\theta_D(\infty)^2 \propto T_m(\infty)$ ,<sup>33</sup> under the assumption that the size in this relation can be extended to  $D$ ,<sup>34,35</sup> there is

$$[\theta_D(D)/\theta_D(\infty)]^2 = T_m(D)/T_m(\infty) \quad (7)$$

Knowing that  $\alpha(T, \infty) \propto 1/E_c(\infty)$  at  $T > \theta_D/2$  and  $E_c(\infty) \propto T_m(\infty)$ ,<sup>35–38</sup> one thus has  $\alpha(T, \infty) \propto 1/T_m(\infty)$ . Extending it into the nanometer regime, we have

$$\alpha(T, D)/\alpha(T, \infty) = T_m(\infty)/T_m(D) \quad (8)$$

According to the first law of thermodynamics, the thermal enthalpy change  $\Delta H$  is given as  $\Delta H = \Delta U + P\Delta V$  where  $\Delta U$  is the internal energy change, and  $P\Delta V$  the work done on the system at a constant pressure  $P$  with  $\Delta V$  being the volume change of the system. As a first-order approximation,  $\Delta V \propto \Delta h$  with  $\Delta h$  denoting the linear change of atomic diameters, which leads to  $P\Delta V \propto \Delta h$ . As derived by Levy,<sup>39</sup>  $\Delta U \propto \Delta h$ . The above two proportional relations bring about  $\Delta H \propto \Delta h$ . Since  $\Delta h \propto \sigma^2$ ,<sup>29</sup>  $\Delta H \propto \sigma^2$ , leading to  $C_p(T, \infty) = \partial H(T, \infty)/\partial T \propto \partial \sigma(T, \infty)^2/\partial T$ . On the basis of the Debye's theory,<sup>40</sup>  $\sigma(T, \infty)^2 \propto T/\theta_D(\infty)^2$  at  $T > \theta_D/2$ . Hence,  $C_p(T, \infty) \propto 1/\theta_D(\infty)^2$ . Assuming that this relationship is still valid in the nanometer regime,  $C_p(T, D)/C_p(T, \infty) = \theta_D(\infty)^2/\theta_D(D)^2$ . In terms of eq 7, it reads

$$C_p(T, D)/C_p(T, \infty) = T_m(\infty)/T_m(D) \quad (9.1)$$

Alternatively,  $C_p(T, D)$  can be traditionally modeled in terms of the Maxwell's derivation for the thermodynamic equation,  $C_p(T, \infty) = C_v(T, \infty) + 9B(T, \infty)V_s\alpha(T, \infty)^2T$  where  $C_v(T, \infty)$  is the specific heat at constant volume and  $B(T, \infty)$  is the bulk modulus.<sup>41</sup>  $C_v(T, \infty)$  can be given with the Einstein's model of  $C_v^E(T, \infty) = 3R[\theta_E(T, \infty)/T]^2 e^{\theta_E(T, \infty)/T}/(e^{\theta_E(T, \infty)/T} - 1)^2$  or the Debye's model of  $C_v^D(T, \infty) = 9R[T/\theta_D(T, \infty)]^3 \int_0^{\theta_D(T, \infty)/T} e^{-x}x^4/(e^x - 1)^2 dx$ .<sup>42</sup> Extending the above functions into the nanometer size,  $C_p(T, D)/C_p(T, \infty) = [C_v(T, D) + 9B(T, D)V_s\alpha(T, D)^2T]/[C_v(T, \infty) + 9B(T, \infty)V_s\alpha(T, \infty)^2T]$ . Since the size-dependence of  $B(T, D)$  is weak especially when  $T$  is far from 0 K and  $T_m$ ,  $B(T, D) \approx B(T, \infty)$ .<sup>43</sup> In light of this approximation and eq 8,  $C_p(T, D)$  is modified as  $C_p(T, D)/C_p(T, \infty) = [C_v(T, D) + 9B(T, \infty)V_s\alpha(T, \infty)^2T_m(\infty)^2/T_m(D)^2]/[C_v(T, \infty) + 9B(T, \infty)V_s\alpha(T, \infty)^2T]$ . In light of  $C_v(T, \infty) = 3\alpha(T, \infty)B(T, \infty)V_s\xi$  with  $\xi$  being the Grüneisen constant,<sup>41</sup> extending it into the nanometer regime, one gets  $C_v(T, D)/C_v(T, \infty) = \alpha(T, D)B(T, D)/\alpha(T, \infty)B(T, \infty)$ . By invoking the above relation  $B(T, D) \approx B(T, \infty)$  and eq 8, one thus has  $C_v(T, D)/C_v(T, \infty) = T_m(\infty)/T_m(D)$ . Substituting it into the above modified  $C_p(T, D)$  equation, it thus says

$$\frac{C_p(T, D)}{C_p(T, \infty)} = \frac{C_v(T, \infty) T_m(\infty) T_m(D) + 9B(T, \infty) \alpha(T, \infty)^2 V_s T_m(\infty)^2}{[C_v(T, \infty) + 9B(T, \infty) \alpha(T, \infty)^2 V_s] T_m(D)^2} \quad (9.2)$$

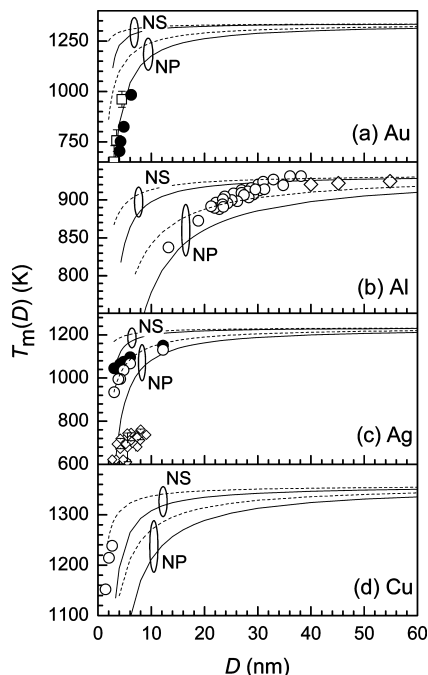


**Figure 1.** Our predictions of  $T_m^{\text{NS}}(D)$  [eq 5, solid curves] and Gibbs–Thomson equations [eq 6, dashed curves] as a function of  $D$  for (a) Au, (b) Al, (c) Ag, and (d) Cu, where the case of NPs is also given for comparison with eqs 3 and 2 with  $d = 0$ . The symbols show experimental or simulation results. (a)  $\square^9$  and  $\bullet^{57}$  are for Au NPs; (b)  $\circ^{58}$  and  $\diamond^{59}$  are for Al NSs; and (c)  $\circ$  is for Ag NPs, and  $\bullet$  is for Ag NSs.<sup>7</sup>  $\diamond^{59}$  is for Ag NPs, and (d)  $\circ$  is for Cu NSs evaluated in light of  $T_m(D)/T_m(\infty) = [\theta_D(D)/\theta_D(\infty)]^2 = \gamma(D)/\gamma(\infty)^{34,60}$  with measured  $\gamma(D)$  from ref 61. Other parameters are from Table 1.

### 3. Results and Discussion

Figure 1 shows  $T_m^{\text{NS}}(D)$  functions in terms of eq 5 or the extended Gibbs–Thomson equation of eq 6 for several metals.  $T_m^{\text{NP}}(D)$  functions of eqs 3 and 2 are also plotted for a comparison purpose.  $T_m^{\text{NS}}(D)$  and  $T_m^{\text{NP}}(D)$  decrease on lowering  $D$  to  $D_0$  where  $T_m^{\text{NP}}(D) < T_m^{\text{NS}}(D) < T_m(\infty)$ . An obvious drop in  $T_m^{\text{NS}}(D)$  occurs at about  $D \approx 5$  nm, although that of  $T_m^{\text{NP}}(D)$  happens at around  $D \approx 10$  nm. Noticeably, such dependence is ascribed to the increase in the surface/volume ratio.<sup>44,45</sup> The weaker dropping

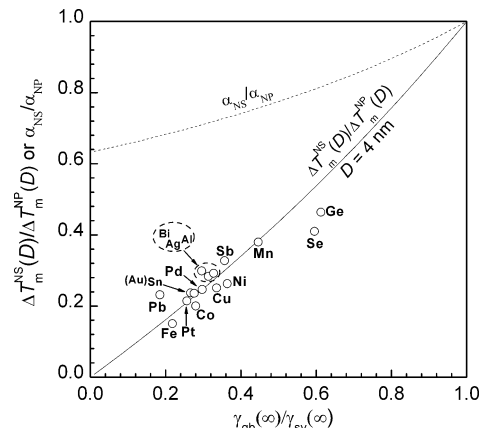


**Figure 2.**  $\Delta T_m^{\text{NS}}(D)/\Delta T_m^{\text{NP}}(D) = [T_m^{\text{NS}}(D) - T_m(\infty)]/[T_m^{\text{NP}}(D) - T_m(\infty)]$  as a function of  $\gamma_{\text{gb}}(\infty)/\gamma_{\text{sv}}(\infty)$  with  $D = 4$  nm in light of eqs 5 and 3 shown as  $\circ$  for 16 elements listed in Table 1, where the solid curve represents an averaged case with  $S_{\text{vib}} = 7.251 \text{ J mol}^{-1} \text{ K}^{-1}$  and  $D_0 = 1.649$  nm as mean values among 16 elements. The dashed curve shows the plot of  $\alpha_{\text{NS}}/\alpha_{\text{NP}}$  as a function of  $\gamma_{\text{gb}}(\infty)/\gamma_{\text{sv}}(\infty)$  in light of the aforesaid relation of  $\alpha_{\text{NS}}/\alpha_{\text{NP}} = 1/[\gamma_{\text{gb}}(\infty)/\gamma_{\text{sv}}(\infty) + [1 - \gamma_{\text{gb}}(\infty)]\gamma_{\text{sv}}(\infty)/\alpha_{\text{NP}}]$ .  $d = 0$  and other parameters are given in Table 1.

rates of  $T_m^{\text{NS}}(D)$  than that of  $T_m^{\text{NP}}(D)$  are induced by the fact that  $\gamma_{\text{gb}} < \gamma_{\text{sv}}$ . When  $D > 10$  nm for NSs or  $D > 20$  nm for NPs, the values of  $T_m^{\text{NS}}(D)$  and  $T_m^{\text{NP}}(D)$  are similar to that of  $T_m(\infty)$ . This result confirms that for larger size, the Gibbs–Thomson equation is valid, where the most bulk thermodynamic amount can be used without big error.

$T_m(D)$  with  $D < 10$  nm assessed by the Gibbs–Thomson equations of eqs 2 and 6 is higher than that of our models of eqs 3 and 5. In essence, the absolute  $E_c$  value of the interior atoms decreases as  $D$  drops,<sup>46</sup> but this fact was not considered in the Gibbs–Thomson equation established for larger  $D$ , for which this phenomenon is not evident. Our predictions agree reasonably well with both experimental and computer simulation results, closing to true situations. Note also that a downward deviation of the measured  $T_m^{\text{NS}}(D)$  from our predictions is observed for Al when  $D < 30$  nm. Such a deviation is related to the elastic energy stored in Al NSs, although it could be annihilated by annealing at elevated temperatures.<sup>47,48</sup>

**TABLE 1: The Relevant Data Used in the Calculations**

	$h(\infty)^{53}$ (nm)	$T_m(\infty)^{54}$ (K)	$S_{\text{vib}}(\infty)^{53 a}$ ( $\text{J mol}^{-1} \text{ K}^{-1}$ )	$\gamma_{\text{sv}}(\infty)^{26}$ ( $\text{J m}^{-2}$ )	$\gamma_{\text{gb}}(\infty)^{26 b}$ ( $\text{J m}^{-2}$ )	$\theta_D(\infty)$ (K)	$\alpha(T, \infty)^c$ ( $10^{-5}/\text{K}$ )
Au	0.288	1337.58	7.620	1.500	0.400		
Al	0.286	933.25	9.650	1.160	0.380		
Ag	0.289	1234	7.820	1.250	0.392		
Cu	0.256	1357.6	7.850	1.790	0.601	343 <sup>54</sup>	1.5
Co	0.251		7.920	2.520	0.706	395 <sup>12</sup>	
Ni	0.249		8.110	2.380	0.866		
Pd	0.275		7.220	2.120	0.630		
Pt	0.278		7.800	2.920	0.749		
Pb	0.350		6.650	0.600	0.111		
Mn	0.273		7.930	1.650	0.736		
Fe	0.248		6.820	2.420	0.528	388 ( $\alpha$ ) <sup>63</sup> 470 ( $\beta$ ) <sup>62</sup>	0.92
Sn	0.281		9.220	0.649	0.179		
Sb	0.290		7.800	0.715	0.255		
Bi	0.309		3.762	0.595	0.176		
Ge	0.245		4.598	0.800	0.490		
Se	0.230	494	5.240	0.132	0.079	135.5 <sup>65</sup>	3.7 <sup>54</sup>

<sup>a</sup> For Sb, Bi, and Ge, the  $S_{\text{vib}}(\infty)$  values are taken from ref 55. For the semiconductor element of Se,  $S_{\text{vib}}(\infty) = S_m(\infty) - R,^{29}$  where  $S_m(\infty) = H_m(\infty)/T_m(\infty)$  with  $H_m(\infty) = 6694 \text{ J/mol}$ .<sup>54</sup> <sup>b</sup> For Se,  $\gamma_{\text{sv}}(\infty) \approx 1.18\gamma_{\text{lv}}(\infty)$ ,<sup>26</sup> where  $\gamma_{\text{lv}}(\infty) = 0.112 \text{ J m}^{-2}$ , denoting the liquid–vapor interface energy.<sup>56</sup> <sup>c</sup> With  $T = 300 \text{ K}$ ,  $\alpha(T, \infty)$  for Cu is averaged by  $1.6 \times 10^{-5}/\text{K}$ <sup>22</sup> and  $1.4 \times 10^{-5}/\text{K}$ ,<sup>48</sup> and that for Fe is given with the extrapolating method.<sup>64</sup>

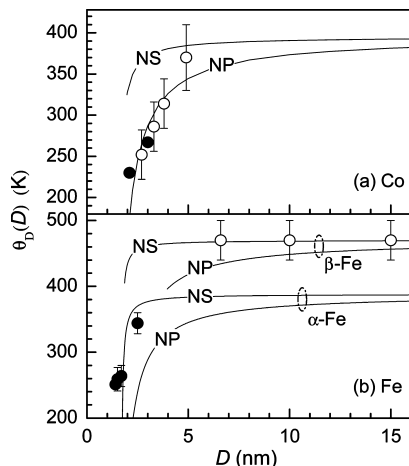


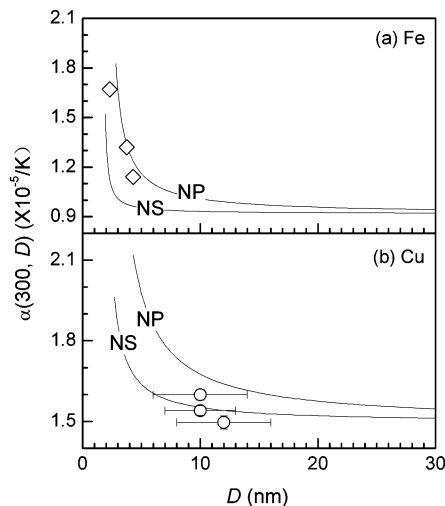
**Figure 3.**  $\theta_D^{\text{NS}}(D)$  functions (curves) in terms of eqs 7 and 5 with  $d = 0$  for (a) Co and (b) Fe where  $\theta_D^{\text{NP}}(D)$  functions in light of eqs 7 and 3 are also given for comparison. The symbols denote the simulation and experimental results: (a)  $\circ$  and  $\bullet$  for Co NPs,<sup>12</sup> (b)  $\circ$  for  $\beta$ -Fe<sup>62</sup> and  $\bullet$   $\alpha$ -Fe<sup>63</sup> embedded in the matrix. Other necessary parameters are shown in Table 1.

In light of eq 5,  $T_m^{\text{NS}}(D)$  is a function of  $\gamma_{\text{gb}}(\infty)/\gamma_{\text{sv}}(\infty)$ . To clarify it further, Figure 2 shows the plot of  $\Delta T_m^{\text{NS}}(D)/\Delta T_m^{\text{NP}}(D) = [T_m^{\text{NS}}(D) - T_m(\infty)]/[T_m^{\text{NP}}(D) - T_m(\infty)]$  as a function of  $\gamma_{\text{gb}}(\infty)/\gamma_{\text{sv}}(\infty)$  at  $D = 4$  nm with the help of eqs 3 and 5. It is observed that  $\Delta T_m^{\text{NS}}(D) < \Delta T_m^{\text{NP}}(D)$  and  $\Delta T_m^{\text{NS}}(D)/\Delta T_m^{\text{NP}}(D)$  is nearly proportional to  $\gamma_{\text{gb}}(\infty)/\gamma_{\text{sv}}(\infty)$ . For the 16 elements listed in Table 1, such as Au, Al, Ag, and Cu,  $0.2 < \gamma_{\text{gb}}(\infty)/\gamma_{\text{sv}}(\infty) < 0.6$ , and the corresponding value range is  $0.15 < \Delta T_m^{\text{NS}}(D)/\Delta T_m^{\text{NP}}(D) < 0.55$ . In fact, the influence of  $\gamma_{\text{gb}}(\infty)/\gamma_{\text{sv}}(\infty)$  on  $\Delta T_m^{\text{NS}}(D)/\Delta T_m^{\text{NP}}(D)$  is realized through  $\alpha_{\text{NS}}/\alpha_{\text{NP}}$ . As shown with the dashed curve for the plot of  $\alpha_{\text{NS}}/\alpha_{\text{NP}}$  as a function of  $\gamma_{\text{gb}}(\infty)/\gamma_{\text{sv}}(\infty)$ ,  $\alpha_{\text{NS}}/\alpha_{\text{NP}}$  decreases as  $\gamma_{\text{gb}}(\infty)/\gamma_{\text{sv}}(\infty)$  is lowered with  $\alpha_{\text{NS}}/\alpha_{\text{NP}} < 1$ . That is, in contrast to NPs, the thermal vibration of atoms at grain boundaries of NSs is suppressed due to the small  $\gamma_{\text{gb}}(\infty)$  value relative to  $\gamma_{\text{sv}}(\infty)$ . Thus, the weakening of the  $\Delta T_m^{\text{NS}}(D)$  function can be scaled by the  $\gamma_{\text{gb}}(\infty)/\gamma_{\text{sv}}(\infty)$  ratio.

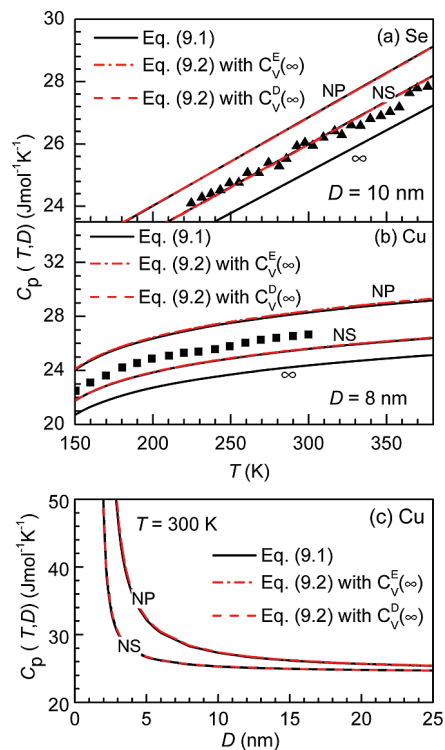
Figure 3 gives the  $\theta_D^{\text{NS}}(D)$  functions of Co and Fe in terms of eqs 7 and 5 in comparison with experimental results.  $\theta_D^{\text{NP}}(D)$  is also plotted in terms of eqs 7 and 3 for comparison. In the figure,  $\gamma_{\text{gb}}(\infty)$  of the Fe/cyanoacrylic resin interface is an averaged value between Fe and the matrix ( $0.015 \text{ J/m}^2$ ).<sup>26</sup>  $\gamma_{\text{gb}}(\infty) \approx \gamma_{\text{sv}}(\infty)/3$  is adopted for  $\text{SiO}_2$  or  $\text{Al}_2\text{O}_3$ , where  $\gamma_{\text{sv}}(\infty) = 0.65 \text{ J/m}^2$  is taken, which is the mean  $\gamma_{\text{sv}}(\infty)$  values of  $\text{SiO}_2$  ( $\sim 0.60 \text{ J/m}^2$ ) and  $\text{Al}_2\text{O}_3$  ( $\sim 0.70 \text{ J/m}^2$ ).<sup>49</sup> It is seen that the  $\theta_D^{\text{NS}}(D)$  decreases with  $D$  and that  $\theta_D^{\text{NP}}(D) < \theta_D^{\text{NS}}(D) < \theta_D(\infty)$ . In contrast to the bulk case, the decrease of  $\theta_D(D)$  with  $D$  arises from the low atomic cohesive energy values at surfaces or grain boundaries because of the extent of coordination imperfection.<sup>50</sup> Because  $\gamma_{\text{gb}}(D) < \gamma_{\text{sv}}(D)$ ,  $\theta_D^{\text{NS}}(D) > \theta_D^{\text{NP}}(D)$ . As shown in the figure, the theoretical formula roughly corresponds to available experimental results.

Figure 4 plots the  $\alpha^{\text{NS}}(T, D)$  functional dependence on  $D$  for (a) Fe and (b) Cu in terms of eqs 8 and 5 in comparison to experimental results.  $\alpha^{\text{NP}}(T, D)$  functions are also shown in light of eqs 8 and 3 for comparison purposes.  $\alpha(T, D)$  increases as  $D$  decreases while the varying rate of  $\alpha^{\text{NS}}(T, D)$  is weaker than that of  $\alpha^{\text{NP}}(T, D)$ . Evidently, this difference related to the atomic thermal vibrational energy at grain boundaries is lower than that on the surface. Our predictions correspond fairly well to available experimental results.

Figure 5 presents  $C_p^{\text{NS}}(T, D)$  and  $C_p^{\text{NP}}(T, D)$  functions on  $T$  for (a) Se and (b) Cu in terms of eqs 9.1 and 9.2 with eq 5 for NSs and eq 3 for NPs in comparison to available experimental



**Figure 4.**  $\alpha^{\text{NS}}(T, D)$  functions (curves) on varying  $D$  in terms of eqs 8 and 5 with  $d = 0$  for (a) Fe and (b) Cu.  $\alpha^{\text{NP}}(T, D)$  functions are also plotted with eqs 8 and 3 for comparison. Symbols: (a)  $\diamond$  denotes the averaged computer simulation result of Fe NPs assessed with cell dimensions at 300–900 K;<sup>64</sup> (b)  $\circ$  is the experimental result of Cu NSs.<sup>48</sup> The necessary parameters are presented in Table 1.



**Figure 5.**  $C_p^{\text{NS}}(T, D)$  functions on varying  $T$  for (a) Se and (b) Cu or on varying  $D$  for (c) Cu in terms of eqs 9.1 (solid curves) and 9.2 [dashed curves for  $C_V^{\text{E}}(T, \infty)$  and dashed-dotted curves for  $C_V^{\text{D}}(T, \infty)$ ] with eq 5 where  $d = 0$ .  $C_p^{\text{NP}}(T, D)$  functions are also plotted using eqs 9 and 3 for comparison. The symbols denote the experimental results with (a)  $\blacktriangle$  for Se NSs<sup>65</sup> and (b)  $\blacksquare$  for Cu NSs.<sup>15</sup> The necessary parameters are shown in Table 1.

results. In the figure,  $C_p(T, \infty) = 17.14 + 0.027T$  for Se,<sup>65</sup> and  $C_p(T, \infty) = 15.95 \times (T - 125.61)^{0.083}$  for Cu.<sup>15,54</sup>  $\theta_E(\infty) = 3\theta_D(\infty)/4$ .<sup>51</sup> The  $V_s$  values are  $7.1 \times 10^{-6} \text{ m}^3/\text{mol}$  for Cu and  $16.45 \times 10^{-6} \text{ m}^3/\text{mol}$  for Se.<sup>54</sup>  $B(T, \infty) = (1.43 - 0.00047T) \times 10^{11} \text{ N m}^{-2}$  for Cu,<sup>52</sup> and  $B(T, \infty) = (0.19 - 0.00038T) \times 10^{11} \text{ N m}^{-2}$  for Se.<sup>54</sup> It shows that the  $C_p(T, D)$  increases with  $T$  and that  $C_p^{\text{NP}}(T, D) > C_p^{\text{NS}}(T, D) > C_p(T, \infty)$  for smaller  $D$ . Compared with the bulk case, the increase in  $C_p(T, D)$  for smaller  $D$  should

be related to larger atomic thermal vibrational energies of atoms at surfaces or grain boundaries. The observation of  $C_p^{NP}(T, D) > C_p^{NS}(T, D)$  is attributed to the fact that the atomic thermal vibrational energy at grain boundaries is smaller than that at surfaces. The model predictions are consistent fairly well with both experimental and computer simulation results. Note that the measured  $C_p^{NS}(T, D)$  values for Cu are observed somewhat higher than our predictions, which can be attributed to the porosity effect or the presence of macroscopic residual stresses in the samples, depending on the processing conditions.<sup>15,47</sup>

The plots of eq 9.1 are overlapped by those of eq 9.2 with both  $C_V^D(T, \infty)$  and  $C_V^E(T, \infty)$ , reflecting that there is little difference between eqs 9.1 and 9.2, or eq 9.1  $\approx$  eq 9.2. The reason for it is that, at  $T < T_m$ , the contribution of the work done by the system at a constant pressure to the enthalpy change is negligibly small with respect to the internal energy change. As a result, in eq 9.2,  $C_V(T, \infty)T_m(\infty)/T_m(D) \gg 9B(T, \infty)V_s\alpha(T, \infty)^2TT_m(\infty)^2/T_m(D)^2$  in the numerator and  $C_V(T, \infty) \gg 9B(T, \infty)V_s\alpha(T, \infty)^2 T$  in the denominator. Equation 9.2 can thus be simplified as  $C_p(T, D)/C_p(T, \infty) \approx T_m(\infty)/T_m(D)$ , which equals eq 9.1.

To see whether  $D$  would bring out a distinction between eqs 9.1 and 9.2,  $C_p(T, D)$  as a function of  $D$  for Cu is typically given in Figure 5c.  $C_p(T, D)$  increases when  $D$  is reduced, with  $C_p^{NP}(T, D) > C_p^{NS}(T, D)$ . An obvious increase in  $C_p^{NS}(T, D)$  occurs at  $D \approx 5$  nm, although that of  $C_p^{NP}(T, D)$  is observed at  $D \approx 10$  nm. When  $D > 10$  nm for NSs or  $D > 20$  nm for NPs,  $C_p(T, D) \rightarrow C_p(T, \infty)$ . Similar to the plots in parts a and b, the difference between eqs 9.1 and 9.2 can hardly be observed.

#### 4. Conclusions

The size-dependences of the melting point, Debye temperature, thermal expansion coefficient, and the heat specific of NSs have been modeled. These functions have a tendency similar to NPs on reducing  $D$ . However, the variation of the above functions for NSs is weaker than that of NPs, whereas this distinction is dominated by the ratio of the grain boundary energy to the surface energy. Our predictions agree fairly well with available experimental or simulation results for semiconductors and metals.

**Acknowledgment.** We acknowledge support by NNSFC (Grants Nos. 60876074 and 50871046) and the National Key Basic Research and Development Program (Grants No. 2010CB631001).

#### References and Notes

- (1) Sun, C. Q. *Prog. Mater. Sci.* **2009**, *54*, 179.
- (2) Gleiter, H. *Acta Mater.* **2000**, *48*, 1.
- (3) Xu, C. X.; Zhu, G. P.; Yang, Y.; Dong, Z. L.; Sun, X. W.; Cui, Y. P. *J. Phys. Chem. C* **2008**, *112*, 13922.
- (4) Di, W. H.; Willinger, M. G.; Ferreira, R. A. S.; Ren, X.; Lu, S. Z.; Pinna, N. *J. Phys. Chem. C* **2008**, *112*, 18815.
- (5) Wu, S. X.; Chu, H. Y.; Xu, H. T.; Wang, X. S.; Yuan, N.; Li, Y. C.; Wu, Z. S.; Du, Z. L.; Schelly, Z. A. *Nanotechnology* **2008**, *19*, 055703.
- (6) Dobruskin, V. K. *Langmuir* **2003**, *19*, 4004.
- (7) Sambles, J. R. *Proc. R. Soc. London A* **1971**, *324*, 339.
- (8) Dick, K.; Dhanasekaran, T.; Zhang, Z. Y.; Meisel, D. *J. Am. Chem. Soc.* **2002**, *124*, 2316.
- (9) Castro, T.; Reifengerger, R.; Choi, E.; Andres, R. P. *Phys. Rev. B* **1990**, *42*, 8548.
- (10) Xiao, S. F.; Hu, W. Y.; Yang, J. Y. *J. Phys. Chem. B* **2005**, *109*, 20339.
- (11) Xiao, S. F.; Hu, W. Y.; Yang, J. Y. *J. Chem. Phys.* **2006**, *125*, 184504.
- (12) Hou, M.; Azaoui, M. E.; Pattyn, H.; Verheyden, J.; Koops, G.; Zhang, G. *Phys. Rev. B* **2000**, *62*, 5117.
- (13) Hong, L. B.; Ahn, C. C.; Fultz, B. *J. Mater. Res.* **1995**, *10*, 2408.
- (14) Zhao, Y. H.; Lu, K. *Phys. Rev. B* **1997**, *56*, 14330.
- (15) Rupp, J.; Birringer, R. *Phys. Rev. B* **1987**, *36*, 7888.
- (16) Hellstern, E.; Fecht, H. J.; Fu, Z.; Johnson, W. L. *J. Appl. Phys.* **1989**, *65*, 305.
- (17) Ruffino, F.; Grimaldi, M. G.; Giannazzo, F.; Roccaforte, F.; Raineri, V. *Nanoscale Res. Lett.* **2008**, *3*, 454.
- (18) Vanithakumari, S. C.; Nanda, K. K. *Phys. Lett. A* **2008**, *372*, 6930.
- (19) Dobruskin, V. K. *J. Phys. Chem. B* **2006**, *110*, 19582.
- (20) Guisbiers, G.; Buchaillet, L. *J. Phys. Chem. C* **2009**, *113*, 3566.
- (21) Yang, C. C.; Li, S. *J. Phys. Chem. C* **2008**, *112*, 16400.
- (22) Eisenmenger-Sittner, C.; Schrank, C.; Neubauer, E.; Eiper, E.; Keckes, J. *Appl. Surf. Sci.* **2006**, *252*, 5343.
- (23) Thomson, J. J. *Applications of Chemical Dynamics*; MacMillan, London, 1888.
- (24) Jones, D. R. H. *J. Mater. Sci.* **1974**, *9*, 1.
- (25) Jackson, C. L.; McKenna, G. B. *J. Chem. Phys.* **1990**, *93*, 9002.
- (26) Jiang, Q.; Lu, H. M. *Surf. Sci. Rep.* **2008**, *63*, 427.
- (27) Liang, L. H.; Zhao, M.; Jiang, Q. *J. Mater. Sci. Lett.* **2002**, *21*, 1843.
- (28) Peters, K. F.; Cohen, J. B.; Chung, Y. W. *Phys. Rev. B* **1998**, *53*, 13430.
- (29) Jiang, Q.; Yang, C. C. *Curr. Nanosci.* **2008**, *4*, 179.
- (30) Jiang, Q.; Shi, H. X.; Zhao, M. *J. Chem. Phys.* **1999**, *111*, 2176.
- (31) Jiang, Q.; Zhang, S.; Zhao, M. *Mater. Chem. Phys.* **2003**, *82*, 225.
- (32) Haiss, W. *Rep. Prog. Phys.* **2001**, *64*, 591.
- (33) Liang, L. H.; Shen, C. M.; Du, S. X.; Liu, W. M.; Xie, X. C.; Gao, H. J. *Phys. Rev. B* **2004**, *70*, 205419.
- (34) Yang, C. C.; Li, S. *Phys. Rev. B* **2007**, *75*, 165413.
- (35) Avramov, I.; Michailov, M. *J. Phys.: Condens. Matter* **2008**, *20*, 295224.
- (36) Shandiz, M. A.; Safaei, A.; Sanjabi, S.; Barber, Z. H. *Solid State Commun.* **2008**, *145*, 432.
- (37) Ruffa, A. R. *Phys. Rev. B* **1977**, *16*, 2504.
- (38) Qi, W. H.; Wang, M. P.; Zhou, M.; Shen, X. Q.; Zhang, X. F. *J. Phys. Chem. Solids* **2006**, *67*, 851.
- (39) Levy R. A. *Principles of Solid State Physics*; Academic: New York, 1968.
- (40) Ziman, J. M. *Principles of the Theory of Solids*, 2nd Ed.; Cambridge University Press: Cambridge, 1976.
- (41) Wagner, M. *Phys. Rev.* **1992**, *45*, 635.
- (42) Ziman, J. M. *Electrons and Phonons*; Oxford University Press: London, 1960.
- (43) Ao, Z. M.; Li, S.; Jiang, Q. *Appl. Phys. Lett.* **2008**, *93*, 081905.
- (44) Guisbiers, G.; Abudukelimu, G.; Wautelet, M.; Buchaillo, L. *J. Phys. Chem. C* **2008**, *112*, 17889.
- (45) Chernyshev, A. P. *Mater. Chem. Phys.* **2008**, *112*, 226.
- (46) Liu, D.; Zhu, Y. F.; Jiang, Q. *J. Phys. Chem. C* **2009**, *113*, 10907.
- (47) Shen, T. D.; Zhang, J. Z.; Zhao, Y. S. *Acta Mater.* **2008**, *56*, 3663.
- (48) Qian, L. H.; Wang, S. C.; Zhao, Y. H.; Lu, K. *Acta Mater.* **2002**, *50*, 3425.
- (49) Overbury, S. H.; Bertrand, P. A.; Somorjai, G. A. *Chem. Rev.* **1975**, *75*, 547.
- (50) Sun, C. Q.; Li, L. C.; Li, S.; Tay, B. K. *Phys. Rev. B* **2004**, *69*, 245402.
- (51) Girifalco, L. *Statistical Mechanics of Solids*; Oxford University Press: Oxford, 2000.
- (52) Lee, E. S.; Lee, S. L.; Jung, K. S.; Kim, I. H. *J. Phys.: Condens. Matter* **1989**, *1*, 9805.
- (53) Lu, H. M.; Wen, Z.; Jiang, Q. *Colloids Surf., A* **2006**, *278*, 160.
- (54) <http://www.efunda.com/materials/elements/>. Accessed July 2009.
- (55) Regel, A. R.; Glazov, V. M. *Semiconductors* **1995**, *29*, 405.
- (56) Keene, B. J. *Int. Mater. Rev.* **1993**, *38*, 157.
- (57) Celestini, F.; Pellenq, R. M.; Bordarier, P.; Rousseau, B. *Z. Phys. D.* **1996**, *37*, 49.
- (58) Eckert, J.; Holzer, J. C.; Ahn, C. C.; Fu, Z.; Johnson, W. L. *Nanostruct. Mater.* **1993**, *2*, 407.
- (59) Révész, Á. *J. Mater. Sci.* **2005**, *40*, 1643.
- (60) Tewary, V. K.; Fuller, E. R. *J. Mater. Res.* **1990**, *5*, 1118.
- (61) Wang, J.; Wolf, D.; Philpot, S. R.; Gleiter, H. *Phil. Mag. A* **1996**, *73*, 517.
- (62) Hayashi, M.; Tamura, I.; Fukano, Y.; Kanemaki, S.; Fujio, Y. *J. Phys. C* **1980**, *13*, 681. Hayashi, M.; Tamura, I. *Surf. Sci.* **1981**, *106*, 453.
- (63) Childress, J. R.; Chien, C. L.; Zhou, M. Y.; Sheng, P. *Phys. Rev. B* **1991**, *44*, 11689.
- (64) Li, X. H.; Ma, M. H.; Huang, J. F. *Chin. J. Chem.* **2005**, *23*, 693.
- (65) Sun, N. X.; Lu, K. *Phys. Rev. B* **1996**, *54*, 6058.